AGU PUBLICATIONS

Geochemistry, Geophysics, Geosystems

RESEARCH ARTICLE
10.1002/2016GC006724

Additive effects of acidification and mineralogy on calcium isotopes in Triassic/Jurassic boundary limestones

Adam B. Jost[1,2], Aviv Bachan[1], Bas van de Schootbrugge[3], Shaun T. Brown[4,5], Donald J. DePaolo[4,5], and Jonathan L. Payne[1]

[1]Department of Geological Sciences, Stanford University, Stanford, California, USA, [2]Department of Earth, Atmospheric, and Planetary Sciences, Massachusetts Institute of Technology, Cambridge, Massachusetts, USA, [3]Marine Palynology and Paleoceanography Group, Department of Earth Sciences, Utrecht University, Utrecht, Netherlands, [4]Department of Earth and Planetary Sciences, University of California, Berkeley, Berkeley, California, USA, [5]Geochemistry Department, Energy Geosciences Division, Lawrence Berkeley National Laboratory, Berkeley, California, USA

Abstract The end-Triassic mass extinction coincided with a negative $\delta^{13}C$ excursion, consistent with release of ^{13}C-depleted CO_2 from the Central Atlantic Magmatic Province. However, the amount of carbon released and its effects on ocean chemistry are poorly constrained. The coupled nature of the carbon and calcium cycles allows calcium isotopes to be used for constraining carbon cycle dynamics and vice versa. We present a high-resolution calcium isotope ($\delta^{44/40}Ca$) record from 100 m of marine limestone spanning the Triassic/Jurassic boundary in two stratigraphic sections from northern Italy. Immediately above the extinction horizon and the associated negative excursion in $\delta^{13}C$, $\delta^{44/40}Ca$ decreases by $\sim 0.8‰$ in 20 m of section and then recovers to preexcursion values. Coupled numerical models of the geological carbon and calcium cycles demonstrate that this $\delta^{44/40}Ca$ excursion is too large to be explained by changes to seawater $\delta^{44/40}Ca$ alone, regardless of CO_2 injection volume and duration. Less than 20% of the $\delta^{44/40}Ca$ excursion can be attributed to acidification. The remaining 80% likely reflects a higher proportion of aragonite in the original sediment, based largely on high concentrations of Sr in the samples. Our study demonstrates that coupled models of the carbon and calcium cycles have the potential to help distinguish contributions of primary seawater isotopic changes from local or diagenetic effects on the $\delta^{44/40}Ca$ of carbonate sediments. Differentiating between these effects is critical for constraining the impact of ocean acidification during the end-Triassic mass extinction, as well as for interpreting other environmental events in the geologic past.

Key Points:
- We observe a large negative calcium isotope excursion above the Triassic/Jurassic boundary.
- Numerical modeling indicates the excursion is too large to be attributed to ocean acidification alone.
- Much of the excursion is due to higher proportions of aragonite in our samples, possibly favored during recovery from acidification.

Supporting Information:
- Supporting Information S1

Correspondence to:
A. B. Jost,
abjost@mit.edu

Citation:
Jost, A. B., A. Bachan, B. van de Schootbrugge, S. T. Brown, D. J. DePaolo, and J. L. Payne (2017), Additive effects of acidification and mineralogy on calcium isotopes in Triassic/Jurassic boundary limestones, *Geochem. Geophys. Geosyst.*, *18*, doi:10.1002/2016GC006724.

Received 8 NOV 2016
Accepted 19 DEC 2016
Accepted article online 29 DEC 2016

1. Introduction

The end-Triassic mass extinction (~201.6 Ma) was one of the five most severe biotic crises of the Phanerozoic [*Raup and Sepkoski*, 1982]. Ocean acidification has been invoked as a kill mechanism based on the preferential loss of heavily calcified marine animals [*Hautmann*, 2006; *Kiessling and Simpson*, 2011; *McRoberts et al.*, 2012] and a decrease in $CaCO_3$ deposition in marine stratigraphic sections [*Hautmann*, 2004]. The extinction is coeval with the emplacement of the Central Atlantic Magmatic Province (CAMP) [*Blackburn et al.*, 2013], an increase in atmospheric pCO_2 [*Schaller et al.*, 2011; *Steinthorsdottir et al.*, 2011], and a negative excursion in the $\delta^{13}C$ of $CaCO_3$ and organic matter [see *Bartolini et al.*, 2012; *Greene et al.*, 2012] suggesting the release of CO_2 from CAMP triggered the loss of marine life. However, the amount of carbon released and the extent of resulting ocean acidification remains poorly quantified. Determining the mass and isotopic composition of carbon release during the end-Triassic mass extinction is critical both to pinpointing the source of carbon and to quantifying the degree of ocean acidification.

Some studies have attempted to constrain release volumes using pCO_2 proxies [*Beerling and Berner*, 2002], but these data have low temporal resolution and may not capture the highest concentrations of pCO_2 that occurred during and immediately after injection. Two recent studies have attempted to accurately replicate the $\delta^{13}C$ record by modeling pulsed releases of CO_2 from CAMP [*Bachan and Payne*, 2015; *Paris et al.*, 2016], but neither study includes model verification using a second geochemical record. Testing extinction scenarios that are constructed to explain carbon isotope data against their predictions for additional isotopes systems is one effective avenue toward better understanding the sequence of events during the Triassic-Jurassic transition.

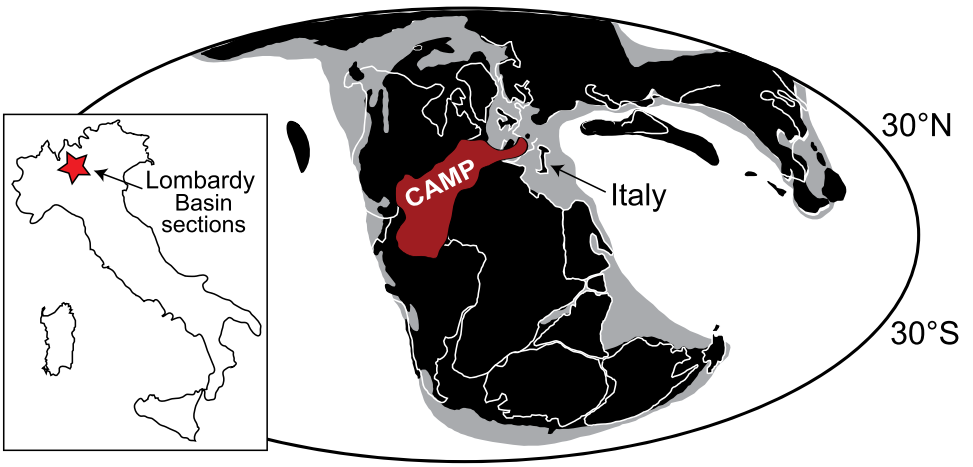

Figure 1. Paleogeographic reconstruction ~200 Ma showing the extent of CAMP and the location of Italy. Inset shows the location of the Lombardy Basin in Italy, where the Val Adrara (45°43′29.33″N, 9°57′32.29″E) and Italcementi (45°46′35.48″N, 9°30′27.09″E) sections are located. Modified from *van de Schootbrugge et al*. [2008] and *Bachan et al*. [2012].

The calcium cycle is linked to the carbon cycle through burial of $CaCO_3$ and dependency between weathering of Ca-bearing minerals and atmospheric pCO_2. Paired $\delta^{13}C$ and $\delta^{44/40}Ca$ records can potentially be used to quantify the amount and composition of carbon required for a negative $\delta^{13}C$ excursion and to test the hypothesis of ocean acidification [*Payne et al*., 2010a; *Komar and Zeebe*, 2011, 2016; *Griffith et al*., 2015]. Under acidification, excess volcanic CO_2 dissolves into seawater, shifting the distribution of dissolved carbonate species away from CO_3^{2-} and decreasing the saturation state of $CaCO_3$ (Ω). $CaCO_3$ precipitation fractionates calcium isotopes and favors ^{40}Ca over ^{44}Ca. As a result, a relative decrease in $CaCO_3$ burial results in less preferential removal of ^{40}Ca from seawater and would cause a negative excursion in $\delta^{44/40}Ca$ beginning at the time of carbon release [*Payne et al*., 2010b]. In addition, increased weathering and seafloor dissolution of $CaCO_3$ as a consequence of high pCO_2 and reduced Ω, respectively, would add isotopically light calcium to seawater. Similarly, $\delta^{13}C$ can be used to place broader constraints on mechanisms underlying $\delta^{44/40}Ca$ variation. Paired data that cannot be explained by any plausible environmental scenario can be used to identify cases in which one or both isotope records are unlikely to represent ancient seawater or atmospheric compositions, but instead reflect degree of influence from local or diagenetic effects.

With the goal of better constraining the nature of carbon release and the severity of ocean acidification, we present new $\delta^{44/40}Ca$ data paired with previously published $\delta^{13}C$ data [*Bachan et al*., 2012, 2014] from samples collected at two sections spanning the end-Triassic extinction and Early Jurassic recovery from the Lombardy Basin in Italy. We then use numerical simulations of CO_2 injection into a coupled model of the carbon and calcium cycles to constrain the mechanisms responsible for $\delta^{13}C$ and $\delta^{44/40}Ca$ variations.

2. Materials and Methods

2.1. Geologic Setting

The Val Adrara and Italcementi sections are located in the Lombardy Basin of northern Italy (Figure 1). The two sections are separated by 35 km, with Val Adrara representing a more distal setting on a shallowly dipping, subtidal ramp. Each section spans approximately 100 m of stratigraphy, including the T/J boundary [*Bachan et al*., 2012]. Facies successions are similar between the two sections. Both sections have previously been studied for sedimentology, paleontology, and $\delta^{13}C$ stratigraphy [see *Bachan et al*., 2012].

Both sections begin in the uppermost Triassic (Rhaetian) Zu limestone, which is composed of algal, molluscan, and coralline packstone and wackestone. Rhaetian fossils, including the Rhaetian pollen taxon *Rhaetipollis germanicus*, last occur in the uppermost Zu limestone and are absent from the overlying Malanotte

Formation (Fm.) [*Galli et al.* 2007]. At these sections, the Malanotte Fm. is interpreted as lowermost Hettangian in age based on the acme of *Kraeuselisporites reissingeri* and the accompanying assemblage of other Hettangian-age pollen taxa [*Galli et al*., 2007]. The base of the Malanotte Fm. contains a marl interval, followed by thinly bedded limestones and alternating shales transitioning upward to shallower facies with more abundant bedforms and carbonate grains by the top of the formation [*Bachan et al*., 2012]. The overlying Albenza Fm. comprises peloidal and oolitic packstone and grainstone with some molluscan material [*Bachan et al*., 2012]. Correlation between the two sections is anchored by the base of the lowermost Jurassic Malanotte Fm. We refined these correlations based on the biostratigraphy of *Galli et al*. [2007] and the $\delta^{13}C$ data of *Bachan et al*. [2012].

2.2. Geochemical Methods

We cut limestone samples using a tile saw and drilled micrite from cut faces for $\delta^{44/40}Ca$ and major/trace element analyses using a bench-top drill press equipped with a 0.8 mm dental drill. Carbonate powders were digested overnight in 1 *M* acetic acid, centrifuged, and separated from the insoluble fraction to avoid contamination from non-carbonate phases such as clays and organic matter. After separation from the insoluble fraction, carbonate samples were dried and redissolved in 3.0 *M* HNO_3. Dissolved samples were then spiked with a ^{42}Ca- and ^{48}Ca-enriched tracer to allow for correction of mass-dependent fractionation occurring during analysis. Typical $^{42}Ca/^{44}Ca$ ratios of spiked samples were 2–3. Calcium was purified from the sample matrix using DGA resin (Eichrom). Samples were loaded on the resin in 3 *M* HNO_3 and the matrix was eluted with subsequent additions of 3 *M* HNO_3 to the column. Calcium was then eluted using DI H_2O, dried down, and treated with concentrated HNO_3 to destroy residual organics from the resin. For each analysis, approximately 3 μg of the purified calcium sample was loaded onto zone-refined Re in a double filament configuration. Samples were run in a Thermo-Fisher Triton multicollector thermal ionization mass spectrometer (TIMS) at the Center for Isotope Geochemistry (CIG), University of California, Berkeley. $\delta^{44/40}Ca$ values are reported relative to Bulk Silicate Earth (BSE) ($^{40}Ca/^{44}Ca = 47.162$ and $^{42}Ca/^{44}Ca = 0.31221$) in standard δ-notation. NIST SRM-915a is $-1.00‰$ on the BSE scale and seawater is $+0.91‰$ [*Nielsen et al*., 2011]. SRM-915A averaged $-1.03‰$ during this study and the long-term reproducibility at CIG is $\sim 0.1‰$.

Concentrations of major and trace elements (Ca, Mg, Mn, and Sr) were measured with an inductively coupled plasma optical emission spectrometer (ICP-OES) in the Environmental Measurements Lab at Stanford University. Carbon isotopes from both sections were measured and presented by *van de Schootbrugge et al*. [2008] and *Bachan et al*. [2012, 2014]. *Bachan et al*. [2012] labeled the initial negative excursion (N1), and two subsequent positive excursions (P1 and P2) in the southern Alps. The N1 and P1 excursions are present within both sections in this study (Figure 2), and the P2 excursion is present at Val Adrara, albeit above our study interval.

3. Results

The two measured sections exhibit similar records of stratigraphic variation in $\delta^{44/40}Ca$ (Table 1 and Figure 2). At Val Adrara, $\delta^{44/40}Ca$ increases from $-0.77‰$ at the base of the section to $-0.45‰$ at the Triassic/Jurassic (T/J) boundary. Just above the boundary, $\delta^{44/40}Ca$ decreases as low as $-1.17‰$ in the Malanotte Fm. $\delta^{44/40}Ca$ then recovers to $-0.39‰$ in the uppermost Malanotte above a stratigraphic gap, and ends at $-0.67‰$ in the lower Albenza Fm. At Italcementi, $\delta^{44/40}Ca$ starts at $-0.89‰$ at the base of the section, increases to $-0.26‰$ before the T/J boundary, and then rapidly decreases to values as low as $-1.13‰$ in the lower Malanotte Fm. The record at Italcementi provides more detail in the upper Malanotte Fm., showing a steady recovery from the nadir up to $-0.46‰$ by the base of the Albenza Fm. The section ends in the lower Albenza at $-0.68‰$. In both sections, the onset of the negative $\delta^{44/40}Ca$ excursion coincides with the N1 excursion in the $\delta^{13}C$ record. The nadir of the $\delta^{44/40}Ca$ excursion occurs approximately 5 m above the peak of the P1 excursion in $\delta^{13}C$.

Stratigraphic variations in [Sr] are also similar between the two sections (Table 1 and Figure 2). Both exhibit uppermost Triassic baseline [Sr] values near 650 ppm (μg/g rock), followed by a sharp rise to $\sim$2800 ppm and a steady decrease back to baseline concentrations in the lower Albenza Fm. The [Sr] and $\delta^{44/40}Ca$ values are inversely correlated at both locations (Val Adrara: Spearman's $\rho = -0.71$, $p = 0.002$; Italcementi: $\rho = -0.76$, $p = 0.001$; see supporting information Table S1 for all correlation coefficients).

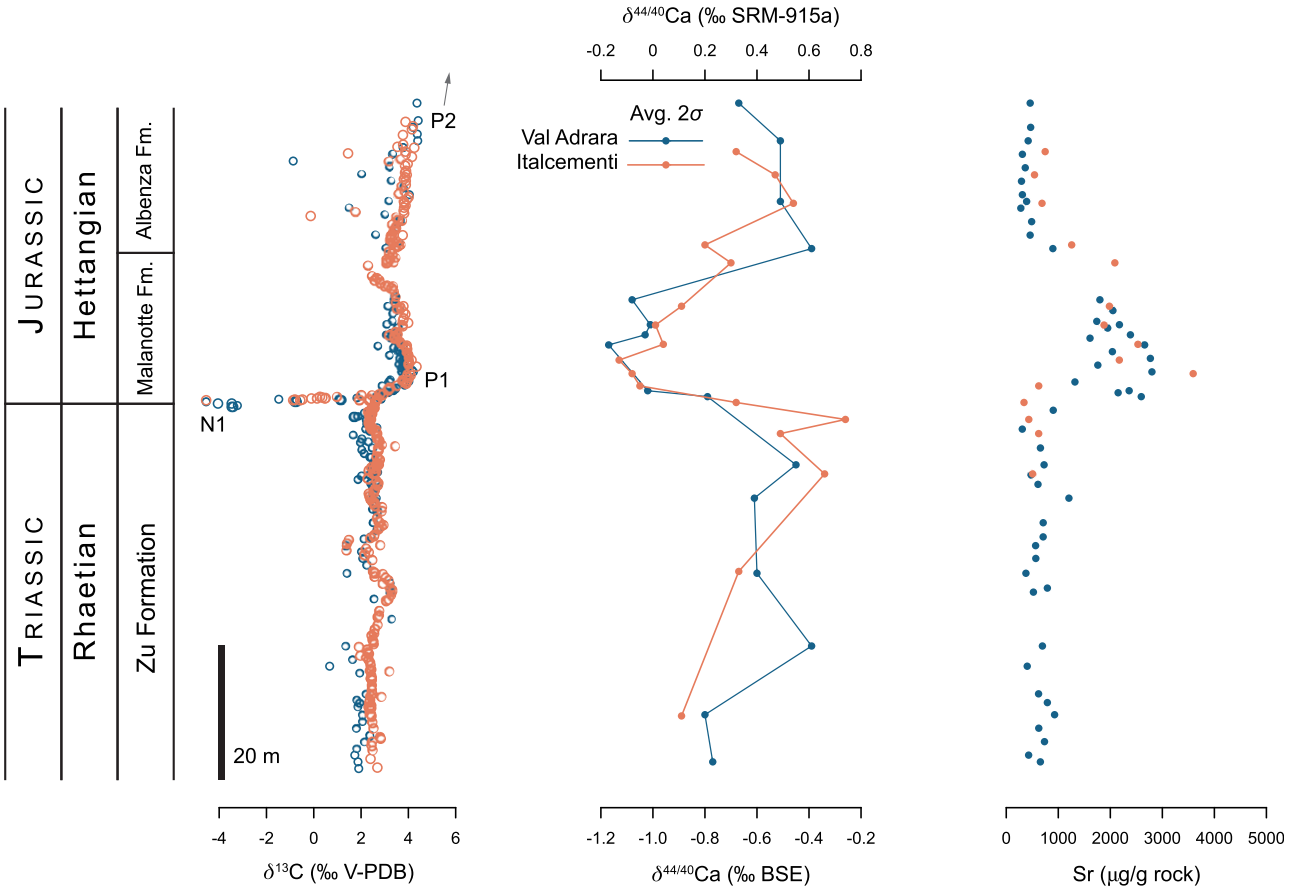

Figure 2. The $\delta^{13}C$, $\delta^{44/40}Ca$, and [Sr] data from each section, exhibiting large excursions immediately above the Triassic/Jurassic boundary. Dark blue is Val Adrara, orange is Italcementi. Val Adrara data are plotted by stratigraphic height, and Italcementi points are minimally adjusted to best match the $\delta^{13}C$ patterns at Val Adrara. Errors on $\delta^{44/40}Ca$ are calculated from replicate measurements of the same sample.

4. Discussion

The co-occurrence of the negative $\delta^{44/40}Ca$ excursion with a rapid negative excursion in $\delta^{13}C$ and the last occurrences of Triassic fossils and the carbonate-poor boundary marl is consistent with an acidification scenario for the mass extinction event. To explore the extent to which acidification can account quantitatively for the coupled variations in $\delta^{44/40}Ca$ and $\delta^{13}C$, we simulated CO_2 injection using a coupled numerical model of the geological carbon and calcium cycles. Our model, similar to one introduced by *Bachan and Payne* [2015], uses mass and isotopic fluxes of carbon and calcium in a single ocean-atmosphere reservoir.

CAMP likely erupted in four pulses [*Schaller et al*., 2011] over the early-middle Hettangian (*spelae-liassicus* zones [*Hillebrandt et al*., 2013]), or potentially into the late Hettangian (*liassicus-angulata* zones [*Hillebrandt et al*., 2013]) based on correlation of $\delta^{13}C$ in northern Italy with geochronologically constrained sections elsewhere [*Bachan and Payne*, 2015]. The interval examined in this study encompasses the N1 and P1 excursions, which likely corresponds to the first observed increase in pCO_2. If the N1 and P1 excursions were associated with first rise in CO_2 observed by *Schaller et al*. [2011, 2012], then our study interval post T/J boundary is likely constrained to 270 kyr. *Bachan and Payne* [2015] modeled this initial eruptive phase using a two-pulse injection (4200 Pg C at $-70‰$ and 14,400 Pg C at $-5.5‰$). In this study, we opt for a single pulse of CO_2 for simplicity.

4.1. Model Construct

We constructed a forward box model of the carbon and calcium cycles to predict the dynamics of these interconnected biogeochemical systems. The ocean is the sole reservoir in our model, in which we track the

Table 1. Geochemical Data From Val Adrara and Italcementi[a]

Stratigraphic Height (m)	$\delta^{13}C$ (‰ VPDB)	$\delta^{18}O$ (‰ VPDB)	Ca (wt %)	Mg (wt %)	Sr (μg/g rock)	Mn (μg/g rock)	$\delta^{44/40}Ca$ (‰ BSE)	$\delta^{44/40}Ca$ (‰ SRM-915a)	$\delta^{44/40}Ca$ (‰ seawater)	2σ for $\delta^{44/40}Ca$	n for $\delta^{44/40}Ca$
Val Adrara											
2.8	1.87	−2.14	31.60	0.66	656	77	−0.77	−1.77	0.14	0.25	3
9.8	2.06	−2.19	31.00	0.57	929	73	−0.80	−1.80	0.11	0.11	2
20.0	1.36	−2.26	31.30	0.67	695	152	−0.39	−1.39	0.52	0.24	2
30.8	1.41	−3.52	29.70	0.66	378	68	−0.60	−1.60	0.31	0.17	2
40.0	2.64	−1.90	32.10	0.47	1204	26	−0.61	−1.61	0.30	0.03	2
46.9	2.54	−2.02	31.40	0.55	727	26	−0.45	−1.45	0.46	0.33	4
57.0	2.76	−2.56	33.67	0.40	2595	126	−0.79	−1.79	0.12	0.21	3
57.9	3.37	−1.68	34.74	0.41	2362	42	−1.02	−2.02	−0.11	0.13	2
64.7	3.79	−2.11	32.30	0.43	2660	74	−1.17	−2.17	−0.26	0.08	2
66.2	3.27	−3.20	35.39	0.32	2386	70	−1.03	−2.03	−0.12	0.16	2
67.7	3.06	−2.94	32.87	0.31	2175	87	−1.01	−2.01	−0.10	0.26	5
71.4	3.37	−2.59	33.20	0.41	1800	54	−1.08	−2.08	−0.17	0.08	2
79.0	3.03	−3.40	35.00	0.56	896	29	−0.39	−1.39	0.52	0.25	3
86.0	3.15	−5.84	35.35	0.66	392	13	−0.51	−1.51	0.40	0.13	2
95.0	4.40	−5.32	34.40	0.16	421	7	−0.51	−1.51	0.40	0.08	2
100.6	4.36	−5.68	33.50	1.29	460	13	−0.67	−1.67	0.24	0.17	2
Italcementi											
7.4	2.44	−1.40	NA	NA	NA	NA	−0.89	−1.89	0.02	0.14	2
23.9	2.50	−1.54	NA	NA	NA	NA	−0.67	−1.67	0.24	0.23	3
35.4	2.51	−1.59	20.30	0.50	507	513	−0.34	−1.34	0.57	0.47	3
41.1	2.68	−4.48	31.03	0.43	623	21	−0.51	−1.51	0.40	0.01	2
43.1	2.42	−2.91	35.98	0.30	433	19	−0.26	−1.26	0.65	0.04	2
45.5	2.58	−1.99	35.79	0.48	341	21	−0.68	−1.68	0.23	0.16	2
47.1	3.49	−1.88	26.08	0.71	624	111	−1.05	−2.05	−0.14	0.11	2
49.9	NA	NA	44.43	0.59	3592	85	−1.08	−2.08	−0.17	0.06	2
53.0	NA	NA	31.09	0.33	2173	38	−1.13	−2.13	−0.22	0.34	2
56.6	3.68	−1.92	39.76	0.41	2531	59	−0.96	−1.96	−0.05	0.11	2
61.0	3.73	−2.19	39.76	0.36	1880	74	−0.99	−1.99	−0.08	0.24	2
65.3	3.79	−2.56	31.26	0.31	1983	47	−0.89	−1.89	0.02	0.23	3
72.9	3.35	−2.14	30.44	0.31	2087	50	−0.70	−1.70	0.21	0.07	2
77.0	3.66	−2.05	35.67	0.59	1257	25	−0.80	−1.80	0.11	0.35	2
86.5	3.83	−2.58	35.76	0.45	687	15	−0.46	−1.46	0.45	0.18	2
93.0	3.93	−3.97	36.52	0.37	543	13	−0.53	−1.53	0.38	0.00	2
98.3	3.88	−6.70	34.89	0.37	748	7	−0.68	−1.68	0.23	0.24	2

[a]For full $\delta^{13}C$ data, see *Bachan et al.* [2012, 2014]. Two sigma values for $\delta^{44/40}Ca$ are calculated from replicate measurements of the same sample. Standard deviations on Ca, Mg, Sr, and Mn measurements based on standard replicate measurements are 0.6 wt %, 0.03 wt %, 1 μg/g rock, and 3 μg/g rock, respectively.

moles of dissolved inorganic carbon (M_C), referred to in the text hereafter as *DIC*, dissolved Ca^{2+} (M_{Ca}), dissolved phosphate (M_P), and dissolved sulfate (M_S). The changes in M_C can be expressed in terms of the major inputs and outputs to the ocean/atmosphere carbon reservoir:

$$\frac{dM_C}{dt} = F_{w,carb} + F_{w,org} + F_{volc} - F_{b,org} - F_{b,carb} \quad (1)$$

where $F_{w,carb}$ and $F_{b,carb}$ are the weathering and burial of calcium carbonate rock, $F_{w,org}$ and $F_{b,org}$ are the weathering and burial of organic carbon, and F_{volc} is the release of volcanic CO_2. We set *DIC* and total alkalinity (*Alk*) to yield an initial pCO_2 value ~2000 ppm and a mean saturation state of calcite, $\Omega_{calcite}$ (herein simply Ω) of 1.75 (see Table 2 for a list of parameters). The changes in M_{Ca} can be expressed similarly:

$$\frac{dM_{Ca}}{dt} = F_{w,sil} + F_{w,carb} - F_{b,carb} \quad (2)$$

where $F_{w,sil}$ is the weathering of Ca-bearing silicate rock. The initial concentration of Ca^{2+} is set to 17 mM, yielding a residence time of approximately 650 kyr (determined as $M_{Ca}/F_{b,carb}$ during steady state). Using equations from *Berner* [2004], we define the non-carbonate weathering fluxes (Ca-silicates and organic C) and carbonate fluxes such that they each scale with the atmospheric pCO_2:

$$F_{w,t} = F_{w,i}(RCO_2)^{GZ}(1 + GZlog(RCO_2))^{0.65} \quad (3)$$

Table 2. Model Parameters and Initial Variables

Variable	Value	Units	References/Notes
T	15	°C	
s	1.035	kg/L	
V_{oc}	2.32×10^{21}	L	
Alk	1.89×10^{-3}	eq/kg	Selected to generate desired *p*CO2 and Ω
DIC	1.90×10^{-3}	mol/kg	Selected to generate desired *p*CO2 and Ω
Initial [Ca]	17×10^{-3}	mol/kg	*Horita et al.* [2002]
Initial [PO4]	25×10^{-6}	mol/kg	Modern concentration
Initial [SO4]	28×10^{-3}	mol/kg	Modern concentration
Initial Ω	1.75		
K_{sp}	4.31×10^{-7}	mol^2/kg^2	Calculated with *Zeebe and Wolf-Gladrow* [2001]
Initial *p*CO2	1893	ppm	*Steinthorsdottir et al.* [2011]
Initial k_{alk}	0.0243		Solved for based on *Alk*, [Ca], and $[SO_4^{3-}]$
Initial $f_{w,org}$	0.25		
Initial $f_{b,org}$	0.25		
F_{volc}	16×10^{12}	mol C/yr	*Kump and Arthur* [1999], adjusted for steady state
Initial $F_{w,carb}$	24×10^{12}	mol CCa/yr	*Kump and Arthur* [1999], adjusted for steady state
Initial $F_{w,org}$	8×10^{12}	mol C/yr	*Kump and Arthur* [1999], adjusted for steady state
Initial $F_{w,sil}$	12×10^{12}	mol Ca/yr	*Kump and Arthur* [1999], adjusted for steady state
Initial $F_{b,carb}$	36×10^{12}	mol CCa/yr	*Kump and Arthur* [1999], adjusted for steady state
Initial C:P, k_{cp}	106		
Initial $F_{b,org}$	12×10^{12}	mol C/yr	*Kump and Arthur* [1999], adjusted for steady state
Initial $F_{w,p}$	11.3×10^{10}	mol P/yr	Derived using $F_{b,org}$ and k_{cp}
Initial $F_{b,p}$	11.3×10^{10}	mol P/yr	Derived using $F_{b,org}$ and k_{cp}
G	3.3		*Berner* [2004]
Z	0.09		*Berner* [2004]
Z_{carb}	0.07		*Berner* [2004]
δ_{volc}	−5.5	‰ VPDB	*Kump and Arthur* [1999], adjusted for steady state
Initial $\Delta_{C,org}$	30	‰	*Kump and Arthur* [1999], adjusted for steady state
Initial $\delta_{b,carb}$	2	‰ VPDB	Based on data from this study
Initial $\delta_{b,org}$	−28	‰ VPDB	*Kump and Arthur* [1999], adjusted for steady state
$\delta_{w,carb}$	2	‰ VPDB	*Kump and Arthur* [1999], adjusted for steady state
$\delta_{w,org}$	−28	‰ VPDB	*Kump and Arthur* [1999], adjusted for steady state
Initial Δ_{Ca}	−1.4	‰	*DePaolo* [2004]
Initial $\delta_{b,Ca}$	−0.3	‰ BSE	Based on data from this study
δ_{riv}	−0.3	‰ BSE	Calculated from relative contributions of F_{wcarb} and F_{wsil}
$\delta_{w,carb}$	−0.4	‰ BSE	*DePaolo* [2004], adjusted for steady state
$\delta_{w,sil}$	−0.1	‰ BSE	*DePaolo* [2004], adjusted for steady state

$$F_{w,carb,t} = F_{w,carb,i}(RCO_2)^{GZ_{carb}}(1 + GZlog(RCO_2)) \tag{4}$$

where G and Z are constant scaling coefficients [see *Berner*, 2004] and RCO_2 is the ratio of CO_2 at time t relative to the level at the initial time i:

$$RCO_2 = \frac{pCO_{2,t}}{pCO_{2,i}} \tag{5}$$

pCO_2 is calculated from the total dissolved inorganic carbon (*DIC*), which is determined from M_C:

$$DIC = \frac{M_C}{sV_{oc}} \tag{6}$$

and alkalinity (*Alk*):

$$Alk = 2\frac{M_{Ca^{2+}}}{sV_{oc}} - 2\frac{M_{SO_4^{2-}}}{sV_{oc}} + k_{alk} \tag{7}$$

where s is salinity, V_{oc} is ocean volume, and k_{alk} is a constant representing the remaining components of alkalinity, which we assume to be fixed during the perturbation. Thus, with *Alk* and *DIC* known, we solve for the other parameters of the carbonate system ($[CO_3^{2-}]$, $[HCO_3^-]$, $[H_2CO_3]$, pCO_2, pH) based on the methods outlined by *Zeebe and Wolf-Gladrow* [2001]. The burial flux of $CaCO_3$ depends on Ω:

$$\Omega = \frac{[Ca^{2+}][CO_3^{2-}]}{K_{sp}} \quad (8)$$

where Ω values <1 imply undersaturation and dissolution, and $\Omega \geq 1$ implies saturation and precipitation. Thus, the burial of carbonate scales with Ω:

$$F_{b,carb,t} = F_{b,carb,i}\frac{\Omega_t - 1}{\Omega_i - 1} \quad (9)$$

Our model does not include a sediment reservoir, so we cannot explicitly dissolve $CaCO_3$ sediment during an acidification. However, if Ω drops below 1.0, $F_{b,carb}$ will become negative and become an input into the ocean reservoir. This process simulates dissolution of $CaCO_3$ in the absence of a dedicated sediment reservoir.

The burial of organic carbon is dependent on the relative changes in the amount of phosphate (M_P), a limiting nutrient on geologic time scales, in seawater:

$$F_{b,org,t} = F_{b,org,i}k_{cp} \quad (10)$$

where k_{cp} is equivalent to the C:P ratio in ocean sediment:

$$k_{cp,t} = k_{cp,i}\left(\frac{M_{PO_4^{2-},t}}{M_{PO_4^{2-},i}}\right)^{p_{cp}} \quad (11)$$

and p_{cp} is a scaling coefficient (assumed to be unity for all scenarios in this study—see *Bachan and Payne* [2015] for other uses). The C:P ratio in sediments is normally Redfieldian (106:1) in oxic conditions, but low oxygen conditions favor release of PO_4^{3-} sorbed on Fe(III) oxides [*Van Cappellen and Ingall*, 1996].

All of the carbon and calcium delivery and removal fluxes can be assigned an average isotopic composition to be used in determining the change in seawater isotopic composition over time:

$$M_C\frac{d\delta_C}{dt} = F_{volc}(\delta_{volc} - \delta_C) + F_{w,org}(\delta_{w,org} - \delta_C) + F_{w,carb}(\delta_{w,carb} - \delta_C) - F_{b,org}(\Delta_{org}) \quad (12)$$

$$M_{Ca}\frac{d\delta_{Ca}}{dt} = (F_{w,sil} + F_{w,carb})(\delta_{w,riv} - \delta_{Ca}) - F_{b,carb}(\Delta_{carb}) \quad (13)$$

where δ_{riv} is the average riverine $\delta^{44/40}$Ca composition, calculated at each t based on the relative contribution of $F_{w,carb}$ and $F_{w,sil}$. We incorporate a carbon injection via a new variable F_{extra} with a δ^{13}C composition δ_{extra}. These are incorporated into equations (1) and (11) such that:

$$\frac{dM_C}{dt} = F_{w,carb} + F_{w,org} + F_{volc} - F_{b,org} - F_{b,carb} + F_{extra} \quad (14)$$

$$M_C\frac{d\delta_C}{dt} = F_{volc}(\delta_{volc} - \delta_C) + F_{w,org}(\delta_{w,org} - \delta_C) + F_{w,carb}(\delta_{w,carb} - \delta_C) - F_{b,org}(\Delta_{org}) + F_{extra}(\delta_{extra} - \delta_C) \quad (15)$$

Initial values and parameters for the model are listed in Table 2. Equations are based on those in *Kump and Arthur* [1999], *Berner* [2004], *DePaolo* [2004], and *Bachan and Payne* [2015]. Select output from a single model run is illustrated in Figure 3.

4.2. Modeling Results and the Role of Acidification in the Excursion

We iteratively modeled a range of CO_2 injection volumes (from 5000 to 60,0000 Pg C), δ^{13}C compositions of injected CO_2 (from $-5‰$ (average mantle) to $-60‰$ (biogenic CH_4)), and durations of CO_2 release (5–50 kyr) assuming seawater [Ca] = 17 m*M* [*Horita et al.*, 2002] (see supporting information for consideration of alternative [Ca] values). We then compared the magnitudes of the modeled negative and positive δ^{13}C excursions to the Val Adrara N1 and P1 δ^{13}C excursions (6.5 below and 2.3‰ above the first sampled δ^{13}C of 1.9‰) to determine the optimum scenario. There are several parameter combinations that can recreate the N1 and P1 excursions; the optimum range is roughly 40,000–45,000 Pg C at $-15‰$ in less than 30 kyr (Figure 4). Importantly, these scenarios result in a negative $\delta^{44/40}$Ca excursion only slightly larger than 0.1‰. In fact, no model scenario within our entire model parameter space produces a $\delta^{44/40}$Ca excursion as large as is observed in our records (maximum modeled excursion is $-0.14‰$; Figure 4). Note that we model

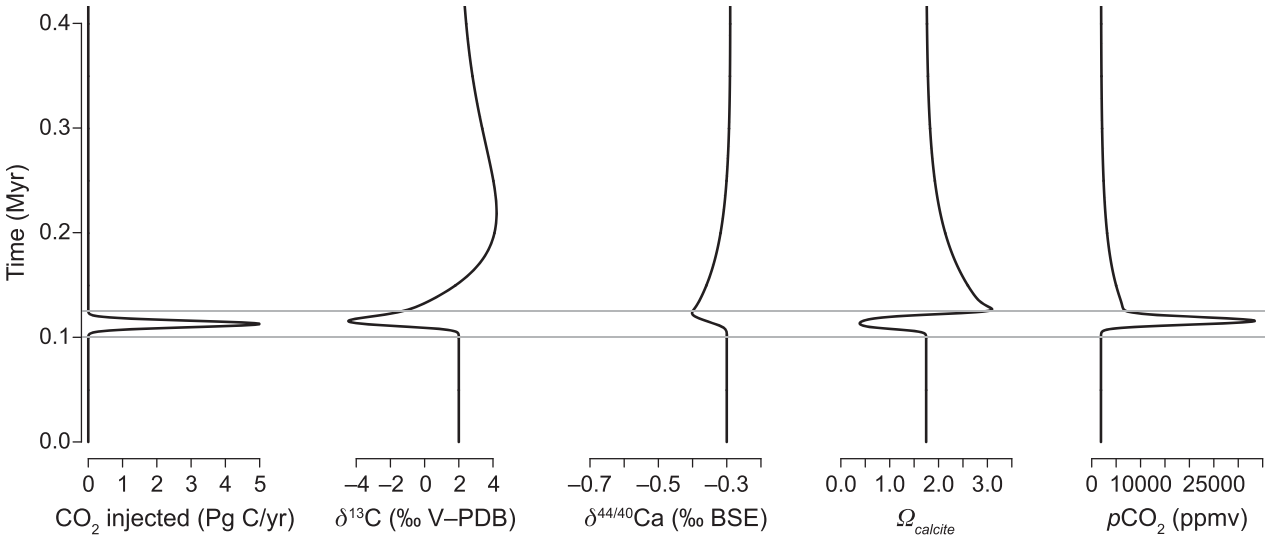

Figure 3. Output from a single model run illustrating the typical geochemical patterns resulting from a CO_2 perturbation in our model. From left to right, rate of CO_2 injection, $\delta^{13}C$, $\delta^{44/40}Ca$, $\Omega_{calcite}$, and pCO_2. This scenario depicts an injection of 40,000 Pg C with a $\delta^{13}C$ value of $-15‰$ injected over 25 kyr. The grey lines signify the start and end of the CO_2 injection.

organic carbon burial with a first-order equation ($p_{cp} = 1$), whereas *Bachan and Payne* [2015] vary p_{cp} between 1 and 3 for different CO_2 pulses. Increasing p_{cp} to 3 would increase the magnitude of the P1 excursion, thereby requiring less CO_2 to yield the same size excursion. Because of this reduction in CO_2 required with increasing p_{cp}, as well as the fact that we are modeling this event as a single CO_2 pulse, our optimum CO_2 magnitudes should be viewed as upper limits. According to our simulations, if the observed excursion in $\delta^{44/40}Ca$ is $-0.72‰$ (based on Val Adrara; it is $-0.87‰$ at Italcementi), then at most 20% of the observed negative excursion in $\delta^{44/40}Ca$ is attributable to CO_2 release and acidification, leaving the remaining 80% to be explained by local or diagenetic mechanisms.

Many processes can influence a $\delta^{44/40}Ca$ record, particularly variation in the magnitude of calcium isotope fractionation ($\Delta^{44/40}Ca$) during $CaCO_3$ precipitation due to precipitation rate [*Tang et al.*, 2008; *DePaolo*, 2011], stoichiometry [*Nielsen et al.*, 2012], mineralogy [*Gussone et al.*, 2005; *Blättler et al.*, 2012], and temperature [*Gussone et al.*, 2005]. Diagenetic processes can also alter the $\delta^{44/40}Ca$ of carbonate sediments and rocks [*Holmden et al.*, 2012; *Fantle*, 2015]. The extent to which one or more of these processes can account for observed $\delta^{44/40}Ca$ variation can be assessed through comparison with predictions under these scenarios. In addition, many scenarios imply predictions for the behavior of other aspects of rock chemistry, such as trace element concentrations.

Submarine groundwater discharge (SGD) can be ruled out as a cause of the T/J boundary $\delta^{44/40}Ca$ excursion at our study site. SGD during marine regression can cause seawater to mix with ^{44}Ca-depleted pore fluids during precipitation and thereby lower its $\delta^{44/40}Ca$ composition [*Holmden et al.*, 2012]. However, the local sea level history is not compatible with this explanation. The lowest $\delta^{44/40}Ca$ values in our data set occur in the Malanotte Fm., which represents a transgression in the Lombardy Basin and much of western Europe [*Galli et al.*, 2007]. The subsequent return to higher $\delta^{44/40}Ca$ values coincides with a transition into the lower Albenza Fm. oolites and peloidal grainstones, which reflect local shallowing after the deposition of the Malanotte Fm. Thus, changes in local base level are in the direction opposite to that expected under an SGD scenario.

The magnitude of $\Delta^{44/40}Ca$ is affected by temperature, precipitation rate (R), and mineralogy. Temperature can be ruled out as the primary control because the observed $\delta^{44/40}Ca$ excursion would require a temperature decrease of approximately 35°C (assuming $0.02‰$/°C [*Gussone et al.*, 2005]), which is unrealistically large and inconsistent with evidence for increased pCO_2 and climate warming [*Schaller et al.*, 2011; *Steinthorsdottir et al.*, 2011].

Precipitation rate is not likely the driver of our $\delta^{44/40}Ca$ record. In laboratory studies, precipitation rates strongly affect the magnitude of $\Delta^{44/40}Ca$ in inorganic calcite [*Lemarchand et al.*, 2004; *Tang et al.*, 2008].

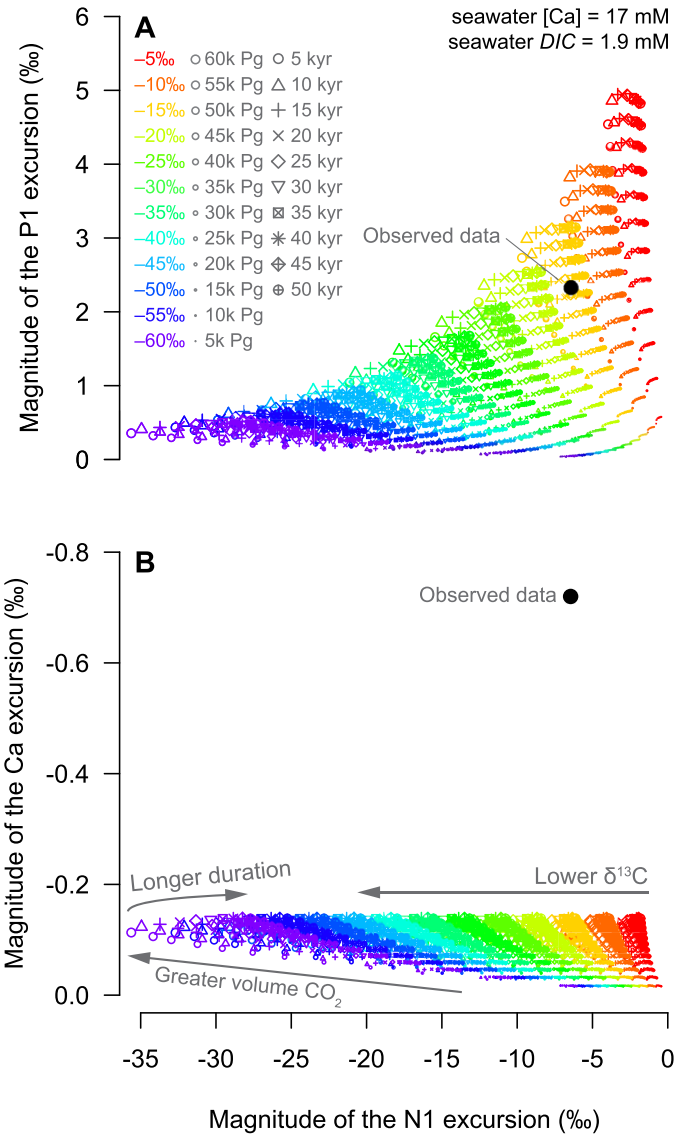

Figure 4. Model predicted (color) and observed (black) values for (a) the N1 and P1 $\delta^{13}C$ excursions and (b) the N1 $\delta^{13}C$ and $\delta^{44/40}Ca$ excursion, demonstrating that while the $\delta^{13}C$ data can be reconciled with modeled scenarios, the $\delta^{44/40}Ca$ data cannot. For the model outputs, symbol size corresponds to the volume of injected CO_2, symbol type corresponds to injection duration, and symbol color corresponds to the $\delta^{13}C$ of the injected CO_2. Model excursion magnitudes are relative to the preevent baseline. Observed $\delta^{13}C$ excursion magnitudes are relative to the first sampled $\delta^{13}C$ value at Val Adrara. The observed $\delta^{44/40}Ca$ excursion magnitude is relative to the last data point (−0.45‰) before the excursion. While there is a range of scenarios that can replicate the $\delta^{13}C$ data, there are no models that can simultaneously replicate the $\delta^{44/40}Ca$ data.

Assuming a constant seawater stoichiometry (Ca^{2+}:CO_3^{2-}), the average $\Delta^{44/40}Ca$ observed for $CaCO_3$ precipitated from modern seawater (~1.4‰) is already close to maximum observed kinetic value, and thus cannot increase in magnitude by more than ~0.2‰ [*DePaolo*, 2011; *Nielsen et al.*, 2012]. Decreasing Ca^{2+}:CO_3^{2-} by orders of magnitude could cause $\Delta^{44/40}Ca$ to increase [*Nielsen et al.*, 2012], however, our model only predicts a decrease of ~40%. Furthermore, it is unclear exactly how this relationship applies to organisms precipitating biogenic $CaCO_3$, as it would require them to vary their forward/backward/net precipitation rates significantly in order to vary $\Delta^{44/40}Ca$ noticeably. It remains unclear whether precipitation rate and/or seawater stoichiometry affected carbonate sediment $\delta^{44/40}Ca$ significantly, but given the required assumptions, we view this scenario as unlikely.

A local increase in the proportion of aragonite (f_a) at our study locations could account for the direction and magnitude of the negative $\delta^{44/40}Ca$ excursion because the $\Delta^{44/40}Ca$ for aragonite is as much as 0.9‰ greater than it is for calcite [*Gussone et al.*, 2005]. The higher [Sr] in the Malanotte samples are also consistent with this scenario, as aragonite incorporates more Sr than high- or low-Mg calcite does. However, this scenario alone does not account for the contemporaneous changes in $\delta^{13}C$. A global switch from calcite to aragonite seas is also a possible cause for the excursion in $\delta^{44/40}Ca$ [*Farkaš et al.*, 2007; *Blättler et al.*, 2012], but the temporary increase in [Sr] is inconsistent with a permanent shift to aragonite. This scenario is also at odds with existing sedimentological and paleontological evidence suggesting the Early Jurassic oceans switched from aragonite to calcite seas [*Hautmann*, 2006; *Stanley*, 2006].

The observed changes in [Sr] are roughly compatible with variable f_a, as calcite has lower concentrations (<1000 ppm) than aragonite does (~7000 ppm) [*Veizer*, 1983]. Predicting how these changes in [Sr] manifested is challenging because f_a (and [Sr]) can vary due to linear mixing of primary aragonite and calcite or

due to preferential diagenetic recrystallization of aragonite to calcite (see supporting information for an extended consideration of $\delta^{44/40}$Ca and [Sr] covariation) [*Husson et al.*, 2015]. An upper limit on changing [Sr] can be determined from a linear mixing; using the concentrations above, increasing f_a by 64% would yield a [Sr] increase of 4000 ppm. This value is greater than the observed maximum [Sr], though some may have been additionally lost during diagenesis [*Brand and Veizer*, 1980]. In either case, all of the $CaCO_3$ in our samples is assumed to be presently calcite, but aragonitic $\delta^{44/40}$Ca and [Sr] values could have been preserved if neomorphism occurred in low-porosity closed system conditions during later diagenesis [*Husson et al.*, 2015].

The majority of the $\delta^{44/40}$Ca excursion in our sections likely represents the recovery from the acidification event (when Ω is greater than background), not the acidification event itself (when Ω is less than background) which may be stratigraphically condensed given the sharpness of the N1 excursion. Other sections are also potentially stratigraphically condensed or even missing this interval given the globally observed decrease in carbonate sedimentation [*Hautmann*, 2004] and that several localities do not capture the N1 excursion [see *Bachan et al.*, 2012; *Greene et al.*, 2012]. Our model predicts that the nadir of $\delta^{44/40}$Ca occurs when Ω is at its maximum (Figure 3). The maximum in Ω would be due to increased delivery of Ca^{2+} via continental weathering as a result of higher pCO_2. Thus, it is possible that aragonite would have been more easily preserved shortly above the main extinction level, when Ω was greatest.

Of the scenarios listed above, local variation in f_a in T/J boundary sediments is the most compatible with our data. Variable f_a has been proposed, in part, as the cause of a large ($\sim$1.2‰), regional-scale negative $\delta^{44/40}$Ca excursion in the Ediacaran-age Wonoka Fm. of south Australia [*Husson et al.*, 2015]. The Wonoka samples exhibit an inverse correlation between $\delta^{44/40}$Ca and [Sr], similarly to the T/J boundary data. However, explaining the T/J boundary $\delta^{44/40}$Ca excursion only by variation in f_a is incomplete. Local variation in mineralogy alone cannot account for the associated mass extinction, the selective loss of heavily calcified marine animals, the large, globally observed excursions in δ^{13}C, or the temporary increase in atmospheric pCO_2. The carbon and calcium cycles are connected through the weathering and burial of $CaCO_3$ and the dependency of weathering on pCO_2. Therefore, if large fluctuations in δ^{13}C during the extinction event were caused by rapid injection of large volumes of CO_2 from CAMP volcanism and the subsequent effects on carbonate saturation and organic carbon production [*Hautmann et al.*, 2008; *Greene et al.*, 2012; *Honisch et al.*, 2012; *Martindale et al.*, 2012], it is likely they also affected seawater $\delta^{44/40}$Ca. Any mineralogical effects on $\delta^{44/40}$Ca would therefore be in addition to primary seawater changes triggered by T/J events.

Given that the effects of acidification and changing mineralogy on $\delta^{44/40}$Ca may be additive, we use our model results to estimate the relative impact of mineralogy on the $\delta^{44/40}$Ca excursion. Assuming $-0.14‰$ of the observed $\delta^{44/40}$Ca excursion was from acidification (20% of the full excursion), $-0.58‰$ would come from increasing f_a. Using an offset of 0.9‰ between calcite and aragonite $\delta^{44/40}$Ca, this corresponds to a 64% increase in f_a during the negative $\delta^{44/40}$Ca excursion.

5. Conclusions

We observe approximately $-0.8‰$ excursion in $\delta^{44/40}$Ca preserved in the lowermost Jurassic limestone sediments in the Lombardy Basin, northern Italy, immediately above the end-Triassic extinction horizon. Numerical modeling of the coupled carbon and calcium cycles demonstrates that the magnitude of the $\delta^{44/40}$Ca excursion is too large to have been caused solely by ocean acidification resulting from emission of volcanic CO_2 during CAMP eruptions. Under a scenario that best explains the δ^{13}C record and the associated evidence for increased pCO_2 and mass extinction, roughly 80% of the T/J $\delta^{44/40}$Ca excursion at our locality is explained by locally higher proportions of aragonite while the remainder reflects the consequences of ocean acidification. Our study demonstrates that a coupled model of the carbon and calcium cycles can be used to deconvolve the contributions of primary seawater isotopic changes and local effects on sedimentary $\delta^{44/40}$Ca.

Acknowledgments
Information on statistics, additional model scenarios, and diagenetic modeling of Sr and $\delta^{44/40}$Ca are available in the supporting information. This study was supported by NASA grant (NNX09AN6767) to J.L.P., by funding from Geological Society of America, the American Association of Petroleum Geologists, the Paleontological Society, and Stanford University McGee Fund to A.B.J., and by the Director, Office of Science, Office of Basic Energy Sciences, Division of Chemical Sciences, Geosciences, and Biosciences, of the U.S. Department of Energy under contract DE-AC02-05CH11231 to D.J.D. The isotopes used in this research were supplied by the United States Department of Energy Office of Science by the Isotope Program in the Office of Nuclear Physics. We thank K. V. Lau, G. Li, K. Maher, T. L. Owens, and K. W. Weaver for their assistance with laboratory work, and two anonymous reviewers for their constructive feedback on this manuscript.

References

Bachan, A., and J. L. Payne (2015), Modelling the impact of pulsed CAMP volcanism on pCO_2 and δ^{13}C across the Triassic–Jurassic transition, *Geol. Mag.*, *153*, 1–19, doi:10.1017/S0016756815000126.

Bachan, A., B. van de Schootbrugge, J. Fiebig, C. A. McRoberts, G. Ciarapica, and J. L. Payne (2012), Carbon cycle dynamics following the end-Triassic mass extinction: Constraints from paired $\delta^{13}C_{carb}$ and $\delta^{13}C_{org}$ records, *Geochem. Geophys. Geosyst.*, *13*, Q09008, doi:10.1029/2012GC004150.

Bachan, A., B. van de Schootbrugge, and J. L. Payne (2014), The end-Triassic negative $\delta^{13}C$ excursion: A lithologic test, *Palaeogeogr. Palaeoclimatol. Palaeoecol.*, *412*, 177–186, doi:10.1016/j.palaeo.2014.07.027.

Bartolini, A., J. Guex, J. E. Spangenberg, B. Schoene, D. G. Taylor, U. Schaltegger, and V. Atudorei (2012), Disentangling the Hettangian carbon isotope record: Implications for the aftermath of the end-Triassic mass extinction, *Geochem. Geophys. Geosyst.*, *13*(1–11), doi: 10.1029/2011GC003807.

Beerling, D. J., and R. A. Berner (2002), Biogeochemical constraints on the Triassic-Jurassic boundary carbon cycle event, *Global Biogeochem. Cycles*, *16*(3), doi:10.1029/2001GB001637.

Berner, R. A. (2004), *The Phanerozoic Carbon Cycle: CO2 and O2*, Oxford Univ. Press, Oxford, U. K.

Blackburn, T. J., P. E. Olsen, S. A. Bowring, N. M. McLean, D. V Kent, J. Puffer, G. McHone, E. T. Rasbury, and M. Et-Touhami (2013), Zircon U-Pb geochronology links the end-Triassic extinction with the Central Atlantic Magmatic Province, *Science*, *340*(6135), 941–945, doi: 10.1126/science.1234204.

Blättler, C. L., G. M. Henderson, and H. C. Jenkyns (2012), Explaining the Phanerozoic Ca isotope history of seawater, *Geology*, *40*(9), 843–846, doi:10.1130/G33191.1.

Brand, U., and J. Veizer (1980), Chemical diagenesis of a multicomponent carbonate system—1: Trace elements, *J. Sediment. Res.*, *50*(4), 1219–1236.

DePaolo, D. J. (2004), Calcium isotopic variations produced by biological, kinetic, radiogenic and nucleosynthetic processes, *Rev. Mineral. Geochem.*, *55*, 255–288.

DePaolo, D. J. (2011), Surface kinetic model for isotopic and trace element fractionation during precipitation of calcite from aqueous solutions, *Geochim. Cosmochim. Acta*, *75*(4), 1039–1056, doi:10.1016/j.gca.2010.11.020.

Fantle, M. S. (2015), Calcium isotopic evidence for rapid recrystallization of bulk marine carbonates and implications for geochemical proxies, *Geochim. Cosmochim. Acta*, *148*, 378–401, doi:10.1016/j.gca.2014.10.005.

Farkaš, J., F. Böhm, K. Wallmann, J. Blenkinsop, A. Eisenhauer, R. Vangeldern, A. Munnecke, S. Voigt, and J. Veizer (2007), Calcium isotope record of Phanerozoic oceans: Implications for chemical evolution of seawater and its causative mechanisms, *Geochim. Cosmochim. Acta*, *71*(21), 5117–5134, doi:10.1016/j.gca.2007.09.004.

Galli, M. T., F. Jadoul, S. M. Bernasconi, and H. Weissert (2005), Anomalies in global carbon cycling and extinction at the Triassic/Jurassic boundary: Evidence from a marine C-isotope record, *Palaeogeogr. Palaeoclimatol. Palaeoecol.*, *216*(3–4), 203–214, doi:10.1016/j.palaeo.2004.11.009.

Galli, M. T., F. Jadoul, S. M. Bernasconi, S. Cirilli, and H. Weissert (2007), Stratigraphy and palaeoenvironmental analysis of the Triassic–Jurassic transition in the western Southern Alps (Northern Italy), *Palaeogeogr. Palaeoclimatol. Palaeoecol.*, *244*(1–4), 52–70, doi:10.1016/j.palaeo.2006.06.023.

Greene, S. E., R. C. Martindale, K. A. Ritterbush, D. J. Bottjer, F. A. Corsetti, and W. M. Berelson (2012), Recognising ocean acidification in deep time: An evaluation of the evidence for acidification across the Triassic-Jurassic boundary, *Earth Sci. Rev.*, *113*(1–2), 72–93, doi: 10.1016/j.earscirev.2012.03.009.

Griffith, E. M., M. S. Fantle, A. Eisenhauer, A. Paytan, and T. D. Bullen (2015), Effects of ocean acidification on the marine calcium isotope record at the Paleocene-Eocene Thermal Maximum, *Earth Planet. Sci. Lett.*, *419*, 81–92, doi:10.1016/j.epsl.2015.03.010.

Gussone, N., F. Böhm, A. Eisenhauer, M. Dietzel, A. Heuser, B. Teichert, J. Reitner, G. Worheide, and W. Dullo (2005), Calcium isotope fractionation in calcite and aragonite, *Geochim. Cosmochim. Acta*, *69*(18), 4485–4494, doi:10.1016/j.gca.2005.06.003.

Hautmann, M. (2004), Effect of end-Triassic CO_2 maximum on carbonate sedimentation and marine mass extinction, *Facies*, *50*(2), 257–261, doi:10.1007/s10347-004-0020-y.

Hautmann, M. (2006), Shell mineralogical trends in epifaunal Mesozoic bivalves and their relationship to seawater chemistry and atmospheric carbon dioxide concentration, *Facies*, *52*(3), 417–433, doi:10.1007/s10347-005-0029-x.

Hautmann, M., M. J. Benton, and A. Tomašových (2008), Catastrophic ocean acidification at the Triassic-Jurassic boundary, *Neues Jahrb. Geol. Paläontol. Abh.*, *249*(1), 119–127, doi:10.1127/0077-7749/2008/0249-0119.

Hillebrandt, A. V., et al. (2013), The Global Stratotype Sections and Point (GSSP) for the base of the Jurassic System at Kuhjoch (Karwendel Mountains, Northern Calcareous Alps, Tyrol, Austria), *Episodes*, *36*(3), 162–198.

Holmden, C., D. A. Papanastassiou, P. Blanchon, and S. Evans (2012), $\delta^{44}/^{40}Ca$ variability in shallow water carbonates and the impact of submarine groundwater discharge on Ca-cycling in marine environments, *Geochim. Cosmochim. Acta*, *83*, 179–194, doi:10.1016/j.gca.2011.12.031.

Honisch, B., et al. (2012), The geological record of ocean acidification, *Science*, *335*(6072), 1058–1063, doi:10.1126/science.1208277.

Horita, J., H. Zimmermann, and H. D. Holland (2002), Chemical evolution of seawater during the Phanerozoic: Implications from the record of marine evaporites, *Geochim. Cosmochim. Acta*, *66*(21), 3373–3756.

Husson, J. M., J. A. Higgins, A. C. Maloof, and B. Schoene (2015), Ca and Mg isotope constraints on the origin of Earth's deepest $\delta^{13}C$ excursion, *Geochim. Cosmochim. Acta*, *160*, 243–266, doi:10.1016/j.gca.2015.03.012.

Kiessling, W., and C. Simpson (2011), On the potential for ocean acidification to be a general cause of ancient reef crises, *Global Change Biol.*, *17*(1), 56–67, doi:10.1111/j.1365-2486.2010.02204.x.

Komar, N., and R. E. Zeebe (2011), Oceanic calcium changes from enhanced weathering during the Paleocene-Eocene thermal maximum: No effect on calcium-based proxies, *Paleoceanography*, *26*, PA3211, doi:10.1029/2010PA001979.

Komar, N., and R. E. Zeebe (2016), Calcium and calcium isotope changes during carbon cycle perturbations at the end-Permian, *Paleoceanography*, *31*, 115–130, doi:10.1002/2015PA002834.

Kump, L. R., and M. A. Arthur (1999), Interpreting carbon-isotope excursions: Carbonates and organic matter, *Chem. Geol.*, *161*, 181–198.

Lemarchand, D., G. J. Wasserburg, and D. A. Papanastassiou (2004), Rate-controlled calcium isotope fractionation in synthetic calcite, *Geochim. Cosmochim. Acta*, *68*(22), 4665–4678, doi:10.1016/j.gca.2004.05.029.

Martindale, R. C., W. M. Berelson, F. A. Corsetti, D. J. Bottjer, and A. J. West (2012), Constraining carbonate chemistry at a potential ocean acidification event (the Triassic–Jurassic boundary) using the presence of corals and coral reefs in the fossil record, *Palaeogeogr. Palaeoclimatol. Palaeoecol.*, *350 352–*, 114–123, doi:10.1016/j.palaeo.2012.06.020.

McRoberts, C. A., L. Krystyn, and M. Hautmann (2012), Macrofaunal response to the end-Triassic mass extinction in the west-Tethyan Kossen Basin, Austria, *Palaios*, *27*(9), 607–616, doi:10.2110/palo.2012.p12-043r.

Nielsen, L. C., J. L. Druhan, W. Yang, S. T. Brown, and D. J. DePaolo (2011), Calcium isotope as tracers of biogeochemical processes, in *Handbook of Environmental Isotope Geochemistry*, edited by M. Baskaran, pp. 105–124, Springer, Berlin.

Nielsen, L. C., D. J. Depaolo, and J. J. De Yoreo (2012), Self-consistent ion-by-ion growth model for kinetic isotopic fractionation during calcite precipitation, *Geochim. Cosmochim. Acta*, *86*, 166–181, doi:10.1016/j.gca.2012.02.009.

Paris, G., Y. Donnadieu, V. Beaumont, F. Fluteau, and Y. Goddéris (2016), Geochemical consequences of intense pulse-like degassing during the onset of the Central Atlantic Magmatic Province, *Palaeogeogr. Palaeoclimatol. Palaeoecol.*, *441*, 74–82, doi:10.1016/j.palaeo.2015.04.011.

Payne, J. L., A. V. Turchyn, A. Paytan, D. J. DePaolo, D. J. Lehrmann, M. Yu, and J. Wei (2010a), Calcium isotope constraints on the end-Permian mass extinction, *Proc. Natl. Acad. Sci. U. S. A.*, *107*(19), 8543–8548, doi:10.1073/pnas.0914065107.

Payne, J. L., A. V. Turchyn, A. Paytan, D. J. DePaolo, D. J. Lehrmann, M. Yu, and J. Wei (2010b), Calcium isotope constraints on the end-Permian mass extinction, *Proc. Natl. Acad. Sci. U. S. A.*, *107*(19), 8543–8548, doi:10.1073/pnas.0914065107.

Raup, D. M., and J. J. Sepkoski (1982), Mass extinctions in the marine fossil record, *Science*, *215*(4539), 1501–1503, doi:10.1126/science.215.4539.1501.

Schaller, M. F., J. D. Wright, and D. V Kent (2011), Atmospheric pCO_2 perturbations associated with the Central Atlantic Magmatic Province, *Science*, *331*(6023), 1404–1409, doi:10.1126/science.1199011.

Schaller, M. F., J. D. Wright, D. V. Kent, and P. E. Olsen (2012), Rapid emplacement of the Central Atlantic Magmatic Province as a net sink for CO_2, *Earth Planet. Sci. Lett.*, *323 324–*, 27–39, doi:10.1016/j.epsl.2011.12.028.

Stanley, S. M. (2006), Influence of seawater chemistry on biomineralization throughout phanerozoic time: Paleontological and experimental evidence, *Palaeogeogr. Palaeoclimatol. Palaeoecol.*, *232*(2–4), 214–236, doi:10.1016/j.palaeo.2005.12.010.

Steinthorsdottir, M., A. J. Jeram, and J. C. McElwain (2011), Extremely elevated CO_2 concentrations at the Triassic/Jurassic boundary, *Palaeogeogr. Palaeoclimatol. Palaeoecol.*, *308*(3–4), 418–432, doi:10.1016/j.palaeo.2011.05.050.

Tang, J., M. Dietzel, F. Böhm, S. J. Köhler, A. Eisenhauer, and M. Dietzel (2008), Sr^{2+}/Ca^{2+} and $^{44}Ca/^{40}Ca$ fractionation during inorganic calcite formation: II. Ca isotopes, *Geochim. Cosmochim. Acta*, *72*(15), 3733–3745, doi:10.1016/j.gca.2008.05.033.

Van Cappellen, P., and E. D. Ingall (1996), Redox stabilization of the atmosphere and oceans by phosphorus-limited marine productivity, *Science*, *271*, 493–496.

van de Schootbrugge, B., J. L. Payne, A. Tomasovych, J. Pross, J. Fiebig, M. Benbrahim, K. B. Föllmi, and T. M. Quan (2008), Carbon cycle perturbation and stabilization in the wake of the Triassic-Jurassic boundary mass-extinction event, *Geochem. Geophys. Geosyst.*, *9*, Q04028, doi:10.1029/2007GC001914.

Veizer, J. A. N. (1983), Chemical diagenisis of carbonates: Theory and application of trace element technique, in *Stable Isotopes in Sedimentary Geology*, chap. 3. [Available at http://scnotes.sepmonline.org/content/sepscsis/1/SEC3.extract.]

Zeebe, R. E., and D. A. Wolf-Gladrow (2001), CO_2 in seawater: Equilibrium, kinetics, isotopes, Elsevier Oceanography Series 65, Amsterdam, 2001, (Paperback) ISBN: 0444509461, *J. Mar. Syst.*, *36*, 269–270, doi:10.1016/S0924-7963(02)00179-3.